Ideal magnetohydrodynamic stability of the tokamak high-confinement-mode edge region

H. R. Wilson, J. W. Connor, A. R. Field, S. J. Fielding, R. L. Miller et al.

Citation: Phys. Plasmas 6, 1925 (1999); doi: 10.1063/1.873492
View online: http://dx.doi.org/10.1063/1.873492
View Table of Contents: http://pop.aip.org/resource/1/PHPAEN/v6/i5
Published by the American Institute of Physics.

Ideal magnetohydrodynamic stability of the tokamak high-confinement-mode edge region*

H. R. Wilson,† J. W. Connor, A. R. Field, and S. J. Fielding
EURATOM/UKAEA Fusion Association, Culham Science Centre, Abingdon, Oxon OX14 3DB, United Kingdom

R. L. Miller, L. L. Lao, J. R. Ferron, and A. D. Turnbull
General Atomics, P.O. Box 85608, San Diego, California 92186

(Received 17 November 1998; accepted 7 January 1999)

The ideal magnetohydrodynamic (MHD) stability of the tokamak edge is analyzed, with particular emphasis on radially localized instabilities; it is proposed that these are responsible for edge pressure gradient limits and edge localized modes (ELMS). Data and stability calculations from DIII-D [to appear in *Proceedings of the 16th International Conference on Fusion Energy*, Yokohama (International Atomic Energy Agency, Vienna, 1998), Paper No. IAEA-F1-CN-69/EX8/1] tokamak equilibria indicate that two types of instability are important: the ballooning mode (driven by pressure gradient) and the peeling mode (driven by current density). The characteristics of these instabilities, and their coupling, are described based on a circular cross-section, large aspect ratio model of the tokamak equilibrium. In addition, preliminary results are presented from an edge MHD stability code which is being developed to analyze general geometry tokamak equilibria; an interpretation of the density threshold to access the high-confinement-mode (H-mode), observed on COMPASS-D [Plasma Phys. Controlled Fusion **38**, 1091 (1996)] is provided by these results. Experiments on DIII-D and the stability calculations indicate how to control ELMs by plasma shaping. © *1999 American Institute of Physics.* [S1070-664X(99)94405-1]

I. INTRODUCTION

The edge region of a tokamak plasma is thought to have a large influence on tokamak performance as a whole, and it is therefore important to develop our understanding of the features which characterize this region. For example, a promising mode of operation is the high-confinement-mode (H-mode), which involves an edge transport barrier, with an associated steep edge pressure gradient. The temperature rises steeply within the transport barrier, up to a so-called ''pedestal'' value, and the overall confinement is sensitive to this value according to some models of the core heat transport.[1] Clearly a steep edge pressure gradient allows a higher temperature pedestal, and improved confinement; however, one is then more vulnerable to pressure-gradient-driven magnetohydrodynamic (MHD) instabilities. The result is that an optimum in tokamak performance is likely to be achieved by a careful balance between good confinement properties and MHD stability. In this paper we discuss some of the issues involved in this optimization.

In the following section we present analyses of DIII-D[2] discharges, which suggest that both the pressure gradient and current density play a role in determining the MHD stability of the plasma edge. Indeed, the current density is likely to be large in the edge of low collisionality H-mode discharges, because of the large bootstrap current density associated with the steep pressure gradient there. In addition, measurements of toroidal mode numbers of precursors to large ELM (edge-localized mode) events suggest that instabilities with moderate to large toroidal mode numbers, up to $n \sim 9$, are responsible for these events on DIII-D.[2] Calculations with the MHD stability code, GATO,[3] for low n are consistent with the higher n modes being more unstable. These facts motivate this study of MHD instabilities with such characteristics. In Sec. III we describe the results of numerical calculations of high n, ideal MHD stability at the edge of a model, large aspect ratio, circular cross-section tokamak. We have developed a code specifically for analyzing edge localized instabilities with moderate to high n in this equilibrium, which provides a simplified model of MHD instabilities, but nevertheless retains the essential features required to describe both ballooning (pressure-driven) and peeling (current-driven) modes (indeed it has similar characteristics to the familiar $s-\alpha$ model[4]). In Sec. IV we describe a new code which performs stability calculations for arbitrary limiter tokamak geometry. The so-called ''ELITE'' code (Edge Localized Instabilities in Tokamak Experiments) shows the same general characteristics for the coupled peeling–ballooning modes as the $s-\alpha$ code, but allows a more quantitative comparison with data. On COMPASS-D[5] it is found that one cannot access the H-mode at low density: an interpretation of this result is provided by the ELITE stability calculations in Sec. V. We summarize in Sec. VI, where we also discuss future work towards a complete model of edge MHD phenomena in tokamaks, and describe experiments performed on DIII-D which show how plasma shaping can provide ELM control.

*Paper K6I1.1 Bull. Am. Phys. Soc. **43**, 1808 (1998).
†Invited speaker.

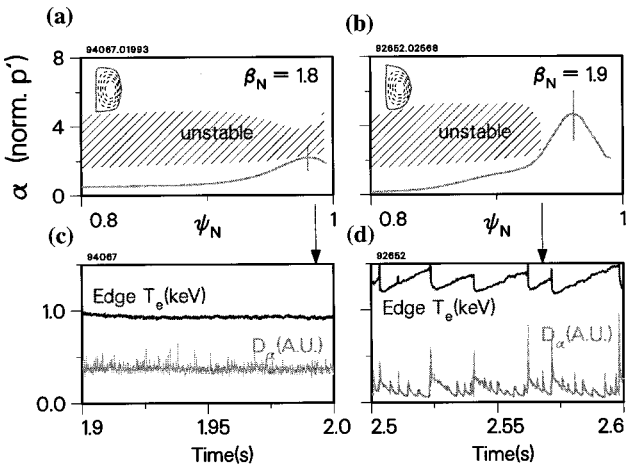

FIG. 1. The profile of the pressure gradient parameter α at the edge of two DIII-D discharges: one confined to the first-stable region (a) and one which has access to second stability (b). Note that the first-stable case has small ELMs, as shown in the D_α trace, with a small effect on the electron temperature (c), while the second-stable case has large ELMs and there is a large fluctuation in edge temperature at each ELM (d). ψ_N is the poloidal magnetic flux, normalized to its edge value.

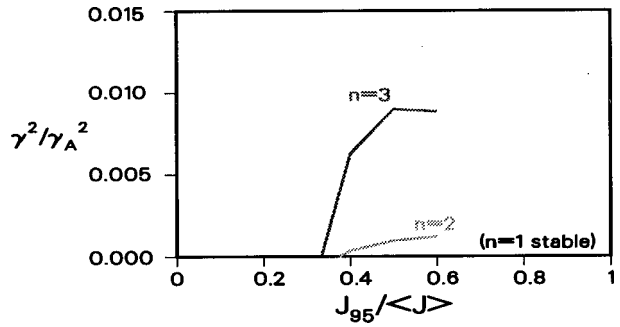

FIG. 2. GATO calculations of MHD stability for low n modes in an equilibrium typical of DIII-D VH modes; the instabilities are driven by edge current density, which is a characteristic of peeling modes.

II. ELM BEHAVIOR ON DIII-D: INTERPRETATION

The cyclic bursts of edge MHD activity, known as ELMs (edge-localized-modes), can be broadly categorized as large, infrequent ''Type I'' ELMs or smaller, more frequent, ''Type III'' ELMs.[6,7] The Type I ELMs are a concern for the next generation of large tokamaks because of the large transient heat loads they can deliver to the divertor target plates, while the smaller Type III ELMs are desirable, as they provide a means to control the plasma density and impurity content, although they tend to lead to a lower edge temperature. Consequently, it is desirable to control the type of ELMs, rather than avoid them. In this section we describe characteristics associated with both ELM types on DIII-D and provide a qualitative interpretation of the results, which points to a means for their control.

The large Type I ELMs appear to be associated with a steep edge pressure gradient, larger than the first stability boundary predicted by ideal $n=\infty$ ballooning theory,[2,8] which has been shown to be applicable at the plasma edge, as well as in the core.[9] An explanation for the high pressure gradient is that the plasma has access to the second stability region as a result of a finite edge current density.[10] Indeed, if one assumes that the edge current density is dominated by the bootstrap current, then this is found to be sufficient to provide second stability access in the discharges where large Type I ELMs are observed.[2] This is illustrated in Fig. 1, comparing two discharges: one is restricted to the low pressure gradient close to the limit predicted by $n=\infty$ ballooning theory, while the second has a high pressure gradient and access to second stability. Note the large ELMs in the second-stable case, and their significant effect on the measured edge electron temperature, while the small ELMs associated with the first-stable discharge have relatively little effect on the measured electron temperature. An interpretation of this will be provided in the next section.

We have argued above that an edge current density, expected to arise from the bootstrap current, is necessary to explain the large pressure gradients measured at the H-mode edge of some DIII-D discharges; what are the effects of this current density and the large edge pressure gradient on the finite n modes? It is well known that at finite n there is an additional drive for MHD modes $\sim J_\parallel'/n$ where $J_\parallel'$ is the radial derivative of the current density parallel to the magnetic field: this drives kink modes. This term can usually be neglected at large n, but to assess its effect at low n we employ the GATO code[3] to investigate the stability of the $n=1$, 2, and 3 ideal MHD modes. Thus, we consider an equilibrium typical of a DIII-D very high confinement ''VH-mode'' discharge and study the stability to low n modes as the edge current density, J_{95}, normalized to the plasma current divided by the cross-sectional area, $\langle J\rangle$, is varied. The result is shown in Fig. 2, where we see that increasing the edge current density destabilizes the higher n modes, with $n=3$ being more unstable than $n=2$ ($n=1$ is stable for all edge current densities considered here); increasing the edge pressure gradient further destabilizes the modes. We learn two things from this study: both pressure gradient *and* edge current density are important drive mechanisms for these instabilities, and the higher n modes tend to be less stable; indeed, toroidal mode numbers of ELM precursors up to $n=9$, with a strong ballooning character, have been measured on DIII-D.[2] From our argument above one might expect higher n current-driven modes to be *more* stable as the current gradient drive is small for these. However, if the current density at the plasma edge is finite, then, as it must be zero in the vacuum, the current density gradient is large and localized at the plasma surface: the result is that the drive $J_\parallel'/n$ remains significant, even at large n. The resulting instabilities are called ''peeling'' modes,[9,11,12] and are localized at the plasma edge; we postulate that these are at least partially responsible for triggering ELMs, and study their properties further in this paper.

In summary, stability analyses and data from DIII-D discharges indicate that moderate-to-high n instabilities, driven by a combination of pressure and current density, are likely to control ELM phenomena and pressure gradient limits at the edge of a tokamak. In the following section we describe the essential features of this class of instability using a code

developed to analyze a large aspect ratio, circular cross-section model tokamak equilibrium.

III. PEELING–BALLOONING MODE PROPERTIES

The conventional ballooning mode formalism[13] is not valid for analyzing the stability of the tokamak edge region because there are inconsistencies in the higher order theory, developed as an expansion in $n^{-1/2}$. Thus, to leading order (the $n\rightarrow\infty$ limit), the conventional ballooning mode theory derives the one-dimensional (1-D) ''ballooning'' equation, which is an eigenmode equation with a ''local'' eigenvalue $\omega^2(\psi,k)$ depending on the radial location, ψ and so-called ballooning phase angle k. Performing a Taylor expansion about the flux surface $\psi=\psi_0$ where ω^2 is a minimum, one can develop the higher order theory: to $O(n^{-1/2})$ one finds that k must be chosen so that ω^2 is minimized; at $O(n^{-1})$, one learns that the ballooning mode is centered on $\psi=\psi_0$, spanning $\sim n^{1/2}$ flux surfaces with a Gaussian envelope and, most importantly, the square of the true mode frequency $\Omega^2=\omega^2(\psi_0)+O(n^{-1})$. The result is that the whole stability and mode structure for the most unstable core ballooning modes can be deduced from the leading order ballooning equation. The situation at the edge is different for two reasons. First, it is usually the case that although the pressure gradient is often largest at the edge of an H-mode discharge, it does not usually achieve a maximum there; when we are restricted to first stability this suggests that, although ω^2 is lowest there, it too will not be a stationary point in general. Second, the ballooning mode radial eigenfunction cannot be a Gaussian centered on the plasma edge, as it would then penetrate the vacuum: the ballooning symmetry (requiring that all rational surfaces spanned by the mode are essentially equivalent) would then be violated. To take account of these special features associated with the plasma edge, we have developed a modified ballooning theory.[9] This assumes that the radial variation of equilibrium parameters is essentially linear at the edge and that the ballooning mode cannot penetrate the vacuum (i.e., the perturbed plasma displacement associated with the instability is assumed to be zero at the plasma boundary). This permits an application of the standard ballooning transformation, followed by an expansion in powers of $n^{-1/3}$. The leading order result yields the standard one-dimensional (1-D) ballooning equation, which is identical to that obtained from the conventional ballooning mode formalism, with the same choice of k forced by the $O(n^{-1/3})$ equation. The $O(n^{-2/3})$ equation predicts an Airy function envelope for the radial mode structure, spanning $\sim n^{1/3}$ rational surfaces. It is in this higher order theory that the modified ballooning theory differs from the conventional ballooning mode theory, and, in particular, one finds that the square of the true mode frequency, Ω^2, differs from the local eigenvalue, ω^2, by $O(n^{-2/3})$.

In summary, we can justify the use of conventional ballooning mode theory to study the plasma edge, described for DIII-D in the previous section. However, we can now use the additional knowledge about the radial structure of ballooning modes to propose an explanation for why large ELMs are experienced in DIII-D when there is access to second stability. The edge ballooning theory predicts that the radial width of the ballooning mode is[9]

$$\Delta r\propto\alpha_d^{-1/3}\left(\frac{\partial\omega^2}{\partial\alpha}\right)^{-1/3}\frac{r}{n^{2/3}}, \tag{1}$$

where r is the minor radius, α is the dimensionless measure of the pressure gradient from high n ballooning theory (defined later) and $\alpha_d=d\alpha/dq$. The size of $\partial\omega^2/\partial\alpha$ depends on whether or not there is second stability access; in particular, when there is no second stability access so that ω^2 is essentially a linear function of α, then $\partial\omega^2/\partial\alpha$ is of order unity and the mode width is simply $\sim r/n^{2/3}$. However, when one is close to second stability access, so that we are close to a minimum of ω^2 with respect to α, then Eq. (1) predicts a much more radially extended mode structure. [Note, close to second stability access there are two marginally stable values of α (i.e., $\omega^2=0$) close to each other, and thus $\partial\omega^2/\partial\alpha$ will be small.] It is natural to assume that a more radially extended instability would lead to a larger heat loss from the plasma so that this provides a possible explanation for the larger ELMs observed on DIII-D when there is access to second stability. We shall return to this when we describe numerical calculations later.

We now turn to the current-driven peeling mode, which is resonant in the vacuum, with its corresponding rational surface close to the plasma surface (in which case the stabilizing effect associated with magnetic perturbations in the vacuum can be neglected).[11] The radially localized nature of the peeling mode allows one to develop an expansion about the plasma surface and derive an accurate expression for a trial function. This leads to a necessary criterion for stability, analogous to the Mercier criterion:

$$\sqrt{1-4D_M}>1+\frac{2}{2\pi q'}\oint\frac{J_\parallel B}{R^2B_p^3}dl, \tag{2}$$

where D_M is the Mercier coefficient ($D_M<1/4$ corresponds to the Mercier criterion for stability[14]), dl is a poloidal arc length element, R is the major radius, B is the magnetic field, B_p is the poloidal magnetic field, q is the safety factor and a prime denotes a differential with respect to the poloidal flux, ψ. We see that large negative D_M (i.e., a ''deep'' magnetic well) is stabilizing: recall that $|D_M|$ increases with increasing pressure gradient, so that pressure is stabilizing for peeling modes, while a finite edge current density is destabilizing; this is the opposite trend to the ballooning mode.

The above analyses are simplifications of the real situation. For example, we assumed that the ballooning mode amplitude is zero at the plasma surface, whereas a more general treatment would allow for the possibility that the instability could couple to modes associated with the vacuum rational surfaces and so tap the free energy associated with the peeling mode. Alternatively, the peeling mode could couple to sideband harmonics resonant in the plasma and have a ballooning nature. To investigate these effects requires a treatment of the full 2-D stability problem: we can no longer make use of ballooning symmetry for the ballooning modes, nor can we make use of the radial localization for

the peeling modes. In the remainder of this paper we address a 2-D calculation of coupled peeling–ballooning mode stability.

The essential features of the coupled peeling–ballooning modes can be illustrated by considering a large aspect ratio, circular cross-section model of the tokamak, analogous to the ''$s-\alpha$'' model. We merely describe the essentials of the system here, and refer the interested reader to Ref. 9. In the limit of large n, stability is determined from a 2-D partial differential eigenvalue equation for the radial component of the perturbed displacement, X. We Fourier expand this in poloidal angle θ:

$$X = e^{-im_0\theta}\sum_m u_m(x)e^{im\theta}, \tag{3}$$

where the radial coordinate $x = m_0 - nq$ ($x=0$ labels the position of the closest vacuum rational surface to the plasma surface) and m is a shifted poloidal mode number. Neglecting terms of $O(n^{-1})$ we derive a set of coupled ordinary differential equations to be solved for the $u_m(x)$:

$$\begin{aligned} &s^2(x-m)^2\frac{d^2u_m}{dx^2} + 2s^2(x-m)\frac{du_m}{dx} - (x-m)^2u_m \\ &-\alpha\left\{ s\left[(x-m)^2+\frac{1}{2}\right]\frac{d}{dx}[u_{m+1}-u_{m-1}] \right. \\ &+ s(x-m)\frac{d}{dx}[u_{m+1}-u_{m-1}] + s(x-m) \\ &\left.\times[u_{m+1}-u_{m-1}] - \frac{1}{2}[u_{m+1}+u_{m-1}] - d_M u_m\right\} \\ &-\frac{\alpha^2}{2}\left\{[(x-m)^2+1]\left(u_m - \frac{1}{2}[u_{m+2}-u_{m-2}]\right)\right. \\ &\left.-(x-m)[u_{m+2}-u_{m-2}]\right\} = 0. \end{aligned} \tag{4}$$

Note that we have introduced an artificial magnetic well through the parameter d_M ($D_M = \alpha d_M/s^2$). The boundary conditions on this set of coupled equations are $u_m(x)\to 0$ in the limit $x\to\infty$, corresponding to the plasma interior, while matching to the magnetic perturbations in the vacuum leads to a set of boundary conditions to be applied at the plasma surface ($x=\Delta$, where $0<\Delta<1$):

$$\begin{aligned} &(\Delta-m)\left\{-s(\Delta-m)\frac{du_m}{dx} - [2-(\Delta-m)]u_m \right. \\ &\left.+\frac{\alpha}{2}(\Delta-m)[u_{m+1}-u_{m-1}]\right\}_{x=\Delta} = \Omega^2 u_m. \end{aligned} \tag{5}$$

Here Ω^2 is an eigenvalue such that $\Omega^2<0$ corresponds to instability (we are interested in marginal stability, for which $\Omega^2=0$). Finally, we represent equilibrium radial profiles through a variation of the pressure gradient parameter, α:

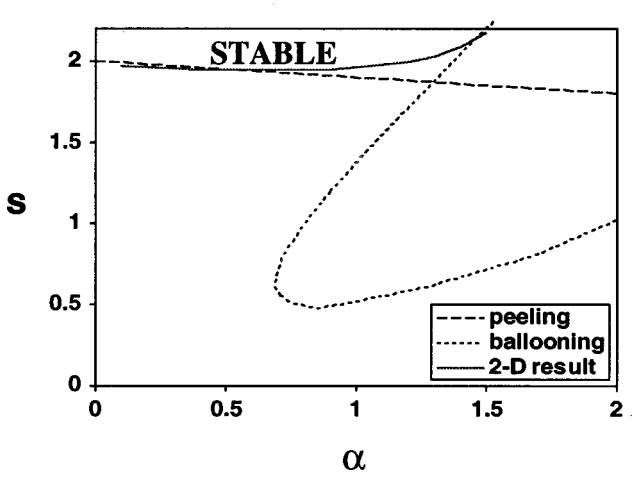

FIG. 3. A modified $s-\alpha$ diagram for coupled peeling–ballooning modes. The dashed curve is the pure peeling mode stability boundary, the dotted curve is the pure ballooning mode stability boundary and the full curve is the boundary predicted by the 2-D stability code. The parameters are $n=20$, $d_M=-0.2$, $\Delta=0.01$, $q=4$.

$$\alpha_a = -2\mu_0\frac{Rq^2}{B^2}\frac{dp}{dr}, \quad \alpha = \alpha_a - \frac{\alpha_d}{n}(x-\Delta), \tag{6}$$

where subscript a indicates the edge value, and α_d represents the strength of the radial variation.

The system of equations (4)–(6) can describe both peeling and ballooning modes. The peeling mode criterion is obtained by performing a local expansion around a single vacuum rational surface, assumed to be very close to the plasma surface (i.e., $\Delta \ll 1$); retaining sideband harmonics, the result is

$$\alpha > \frac{2(2-s)}{-d_M}, \tag{7}$$

for stability. Note that we have expressed the edge current density in terms of the magnetic shear [$s = 2(1 - J_\parallel/\langle J\rangle)$]. The ballooning mode criterion can be obtained by adopting the ballooning approximation $u_m(x) \simeq e^{i(m_0-m)k}u(x-m)$ which yields the modified $s-\alpha$ equation:

$$\frac{d}{d\eta}\left\{[1+h^2(\eta)]\frac{dy}{d\eta}\right\} + \alpha\Gamma y = 0, \tag{8}$$

where η is the ballooning angle, $h(\eta) = s(\eta - k) - \alpha\sin\eta$ and $\Gamma = \cos\eta + h\sin\eta + d_M$. The eigenvalue condition for this equation defines marginal stability contours in the $s-\alpha$ plane, with k to be chosen to maximize the unstable region. The independent variable y is the Fourier transform of u.

It is convenient that the stability of both the peeling and ballooning modes can be represented in terms of the magnetic shear, s, and the normalized pressure gradient α: the stability properties of both modes can therefore be summarized on an $s-\alpha$ diagram. The result for a relatively weak magnetic well, $d_M=-0.2$, is shown in Fig. 3. Also shown on this plot is the result of the 2-D calculation for $n=20$ and a low value of $\Delta=0.01$. We see that the 2-D stability curve follows the peeling mode branch at low α and at higher α

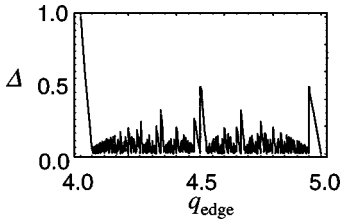

FIG. 4. The minimum value of Δ considering a range of n, $10 \leqslant n \leqslant 20$, plotted as a function of edge safety factor q.

follows the ballooning mode branch. Note that the 2-D result is more stable than the $n=\infty$ ballooning mode result would predict: this has been shown to be a consequence of the finite n stabilizing correction.[9] For larger Δ, the stabilizing effect of the vacuum perturbations on the peeling mode becomes stronger, so that for $\Delta=0.9$ stability is essentially determined solely by the ballooning mode.[15] Indeed, in the limit $\alpha \to 0$ the marginal stability point is at $s=2(1-\Delta)$. This sensitivity to Δ raises the question of how to choose this parameter. To study this we suppose that a range of toroidal mode numbers, $10 \leqslant n \leqslant 20$, could, in principle, be unstable and calculate the minimum Δ as a function of q; this is shown in Fig. 4. Note that there is not much variation as q is varied, and the average value is $\Delta=0.1$; increasing the range to $10 \leqslant n \leqslant 40$ this average falls to 0.05, suggesting that the results for small Δ are likely to be applicable.

Let us return to Fig. 3. We notice that in the absence of the peeling mode, there is access to second stability at sufficiently low magnetic shear. However, this requires a large edge current density, so that the peeling mode is unstable. The result is that it is not possible to gain access to the second stability region for these parameters. Deepening the magnetic well (i.e., making d_M more negative) improves the second stability access by increasing the gradient of the peeling mode stability line [see Eq. (7)], and pushing the ballooning mode boundary up into the top right hand corner of the stability diagram:[15,16] the case for $d_M=-0.6$ is shown in Fig. 5(a), where it can be seen that the pure peeling and ballooning mode unstable regions are now separated, and there exists a window of access to the second-stable region. Figure 5(b) shows the situation for the 2-D coupled mode calculation: we see that for $d_M=-0.6$ the peeling and ballooning modes remain coupled and there is no access to second stability even though the pure ballooning and peeling mode boundaries are well-separated. To regain access to second stability, it is necessary to further deepen the magnetic well, and for $d_M=-0.645$ we see that the peeling and ballooning modes do de-couple to provide a stable window through to second stability.

In Fig. 6 we show the different edge ballooning mode structures for two cases: $d_M=-0.2$ when there is no second stability access, and $d_M=-0.645$ where there is second stability access. Note that when there is second stability access the mode spans many more rational surfaces, in line with the result of the edge ballooning mode analytic calculation given in Eq. (1). Indeed, we see that in both cases the envelope of the amplitude of Fourier harmonics agrees with the Airy function prediction of the edge ballooning mode theory.

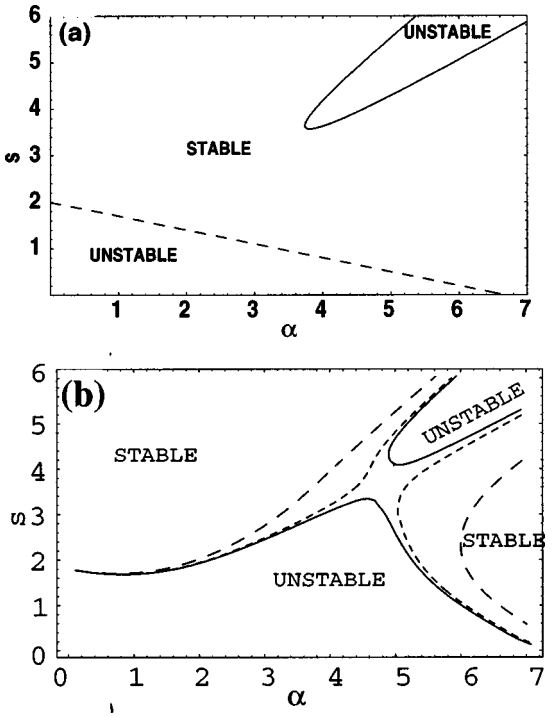

FIG. 5. (a) The effect of a deeper magnetic well ($d_M=-0.6$) on the pure peeling and ballooning modes suggests there is access to the second stability region. However, in (b) we show the results of the 2-D calculation, where it can be seen that the coupling is still strong for $d_M=-0.6$ (dashed curve) and no access to second stability exists; increasing $d_M=-0.64$ (dotted curve) reduces the unstable region, which eventually necks off to provide second stability access for $d_M=-0.645$ (a full curve). The other parameters are as for Fig 3, but $\Delta=0.1$.

IV. EDGE MHD STABILITY IN GENERAL TOKAMAK GEOMETRY

The results of the $s-\alpha$ code are useful to demonstrate the essential features of coupled peeling–ballooning modes, but to make more meaningful comparisons with experimental data it is necessary to develop a more realistic model. This work is under way, and here we present some preliminary results from a new ideal edge MHD stability code, called ELITE, which has an improved treatment of the tokamak geometry.

The ELITE code has the same basic structure as the $s-\alpha$ code, employing a large n ordering to reduce the system to a single 2-D eigenmode equation for the radial component of the plasma displacement, X. This is Fourier decomposed in a straight-field line poloidal angle, ω, and toroidal angle φ:

$$X=\sum_m u_m(x)e^{-im\omega}e^{in\varphi}, \quad \omega=\frac{1}{q}\int^l \frac{fdl}{R^2B_p}, \tag{9}$$

to derive a set of coupled ordinary differential equations of the form

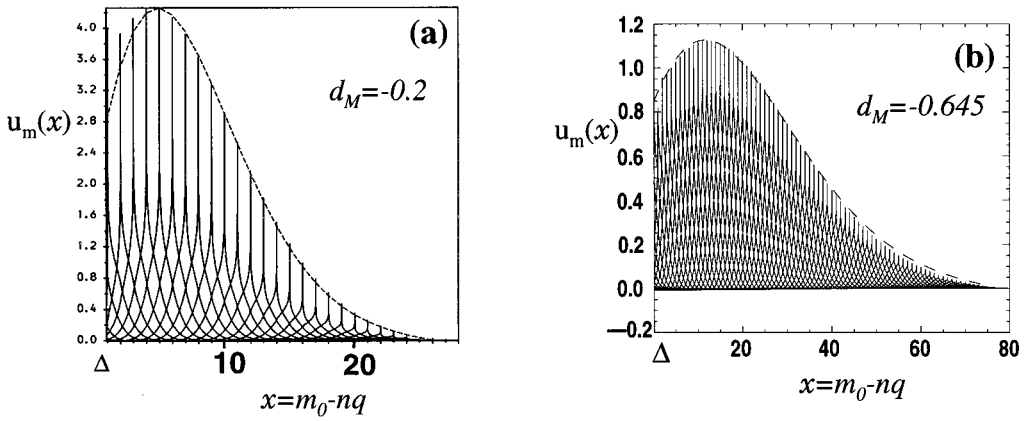

FIG. 6. Radial mode structures for (a) a first-stable ballooning mode case and (b) a second-stable case. The dashed curves correspond to the Airy function envelopes predicted by the modified edge ballooning theory. Parameters are $n=20$, $q=4$.

$$A_3^{m,m'}\frac{d^2u_{m'}}{dx^2}+A_2^{m,m'}\frac{du_{m'}}{dx}+A_1^{m,m'}u_{m'}=0, \tag{10}$$

where the matrix elements $A_i^{m,m'}$ are functions of the radial coordinate x, the poloidal mode number, m and flux surface averages of equilibrium quantities (see the Appendix); a summation over repeated indices is implied. These equations are to be solved subject to the boundary conditions $u_m(x)\to 0$ as $x\to\infty$, while at the plasma–vacuum interface we match to the vacuum perturbations to derive the boundary conditions:

$$(m-nq)\left\{\left[(T_3^{m,m'}-im'T_6^{m,m'})\frac{m'-nq}{nq}-\frac{m'q'}{nq^2}T_4^{m,m'}+f'T_{12}^{m,m'}+fp'T_{13}^{m,m'}\right]u_{m'}-\frac{q'(m'-nq)}{q}T_4^{m,m'}\frac{du_{m'}}{dx}\right\}-n\delta W_{m,m'}^{\mathrm{vac}}u_{m'}+n\Omega^2u_m=0. \tag{11}$$

The matrix elements $T_i^{m,m'}$ are also defined in the Appendix, and $\delta W_{m,m'}^{\mathrm{vac}}$ represents the stabilizing contribution of the energy associated with magnetic perturbations in the vacuum. A separate code has been developed to calculate $\delta W_{m,m'}^{\mathrm{vac}}$ for a given equilibrium, which is a version of a code due to Pletzer,[17] modified to allow a more accurate treatment of high n modes. A linear radial variation of α is assumed, which, for this general geometry case, is defined as

$$\alpha_a=-\frac{2V'}{(2\pi)^2}\left(\frac{V}{2\pi^2R_0}\right)^{1/2}\mu_0p', \quad \alpha=\alpha_a-\frac{\alpha_d}{n}(x-\Delta), \tag{12}$$

where V is the plasma volume, R_0 is the major radius and a prime denotes a derivative with respect to the poloidal flux, ψ.

For this first version of the code the equilibrium is specified in terms of the properties of the last closed flux surface, and an expansion about this flux surface is employed to calculate the equilibrium properties a small distance into the plasma.[18,19] As a result the code can only address edge-localized modes, and this equilibrium expansion fails for the more extended of the ballooning modes. From Eq. (1) we see that we can restrict the radial extent of the ballooning mode by choosing α_d large; this choice also has the effect of increasing the finite n correction to the ballooning mode stability.

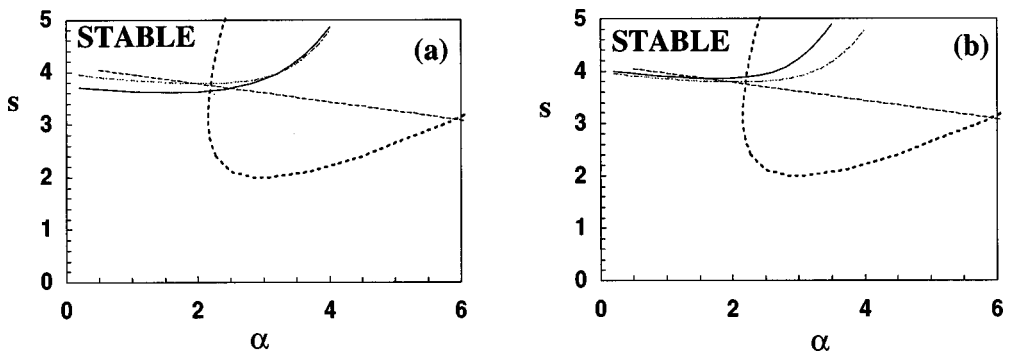

FIG. 7. (a) The pure peeling (dashed) and pure ballooning (dotted) mode marginal stability boundaries compared with the $n=10$ stability results from ELITE for $\Delta=0.1$ (full) and $\Delta=0.05$ (dashed/dotted). This equilibrium has aspect ratio 3.3, elongation 1.6 and triangularity 0.2. In (b) we compare the stability diagrams for $n=10$ (dashed/dotted) and $n=20$ (full) for $\Delta=0.05$; we see the higher n mode is more unstable, particularly at large α: this is expected from the analytic edge ballooning mode theory (Ref. 9).

To benchmark the code, we compare the results of ELITE with the infinite n ballooning calculation and the peeling mode criterion [from Eq. (2)] in Fig. 7. Here we have specified the flux surface shape to be of the form

$$R = R_0 + r\cos\{\theta + [\sin^{-1}\delta]\sin\theta\}, \tag{13}$$

$$Z = r\kappa\sin\theta,$$

where Z is the vertical height above the mid-plane, r is the minor radius on the mid-plane, θ is the geometrical poloidal angle, δ is the triangularity and κ is the elongation. The variation of the poloidal field is then given by[19]

$$\frac{RB_p}{R_0 B_{p0}} = \frac{\kappa^{-1}[\sin^2(\theta + x\sin\theta)(1 + x\cos\theta)^2 + \kappa^2\cos^2\theta]^{1/2}}{\cos(x\sin\theta) + R_0'\cos\theta + [s_\kappa - s_\delta\cos\theta + (1 + s_\kappa)x\cos\theta]\sin\theta\sin(\theta + x\sin\theta)}, \tag{14}$$

where R_0' is the radial derivative of the Shafranov shift and

$$\sin x = \delta, \quad s_\kappa = \frac{r}{\kappa}\frac{d\kappa}{dr}, \quad s_\delta = \frac{r}{\sqrt{1-\delta^2}}\frac{d\delta}{dr}. \tag{15}$$

The plot in Fig. 7(a) is for a moderately shaped equilibrium with $q_a = 3$, aspect ratio $A = 3.3$, elongation $\kappa = 1.6$, and triangularity $\delta = 0.2$. If a relatively large value of $\Delta = 0.1$ is chosen, this increases the stabilizing effect of the magnetic perturbations in the vacuum on the peeling mode, as can be seen from the 2-D results at low α in the figure. If Δ is reduced, then the stabilizing effect of the vacuum is reduced, as it was in the case for the $s - \alpha$ curves; Figure 7(a) also shows the ELITE result for $\Delta = 0.05$ for comparison. As α increases, the result from ELITE tracks the peeling mode criterion until α approaches the ballooning boundary. It then tracks the ballooning mode boundary, but is significantly more stable than the $n = \infty$ ballooning analysis would suggest; this is a consequence of the relatively low value chosen for $n = 10$ and the large value of α_d. Figure 7(b), which compares the result for $n = 10$ with that for $n = 20$ (for $\Delta = 0.05$), supports this; note that the higher n destabilizes the ballooning mode, placing the marginal stability boundary closer to the pure ballooning stability boundary, but has relatively little effect on the peeling mode (the opposite to the effect of varying Δ). This is expected from the analytic theory.[9]

V. IMPLICATIONS FOR H-MODE ACCESS IN SMALL TOKAMAKS

Previously we have postulated that instability to the peeling mode in H-mode discharges prevents small tokamaks entering the H-mode at low density.[15,20] For example, in low density, electron cyclotron resonance heated COMPASS-D discharges the H-mode cannot be achieved, even though the input power is many times higher than that which is predicted from the International Thermonuclear Experimental Reactor (ITER)[21] H-mode power threshold scaling laws.[22] The argument was based upon a large aspect ratio, circular flux surface model of the tokamak, in which the bootstrap current destabilizes the peeling mode when the pressure gradient is large, and the collisionality is low. We can use the ELITE code to test this model for a more realistic geometry, typical of COMPASS-D high field (2.1 T) discharges. The stability diagram is shown in Fig. 8 for COMPASS-D parameters, choosing a low value $\Delta = 0.05$. There are no measurements of the current density on COMPASS-D, so an estimate of the magnetic shear is problematic. However, if we assume that all the current at the plasma edge is provided by the bootstrap current, then the shear is linearly related to the pressure gradient parameter α. This relation is shown by the dotted curve for a low collisionality discharge ($\nu_* = 0.67$), which would not be expected to achieve a H-mode, and by the dashed curve for a higher collisionality discharge ($\nu_* = 1.7$), in which one would expect to achieve a H-mode with sufficient heating power. We have defined the collisionality:

$$\nu_* = 1.2\times 10^{-3}\frac{n_{19}R_o q}{T_e^2\epsilon^{3/2}}, \tag{16}$$

where n_{19} is the density measured in 10^{19} m^{-3}, T_e is the temperature in keV and ϵ is the inverse aspect ratio. The experimental results, obtained by optical spectroscopy with a helium beam, the HELIOS system,[23] are shown in Fig. 9: L-modes are indicated by the squares; H-modes with no ELM observed during data sampling are indicated by the triangles, and H-mode with an ELM occurring during data sampling, are shown by the diamonds. We see that the H-mode is indeed limited to high collisionality, and furthermore there are more ELMs as one approaches low collisionality. In terms of the stability diagram shown in Fig. 8, this has the following interpretation. At high collisionality the pressure gradient can rise without any significant increase in the bootstrap current (along the dashed line), so that the peeling mode remains stable. However, at lower collisionality (along the dotted line) the peeling mode is destabilized when α exceeds some critical value: as the H-mode is usually associated with higher α values, this may explain why the H-mode cannot be accessed in low density COMPASS-D discharges. In larger, hotter tokamaks the current would be expected to diffuse more slowly than the pressure, so that transiently the edge could remain stable, even at high α and low collisionality. Of course, the current would diffuse eventually, resulting in the peeling mode being destabilized and a burst of energy from the plasma edge; one might therefore

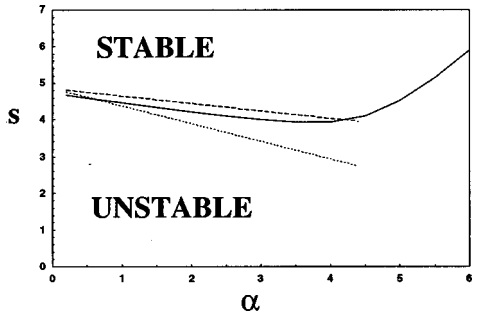

FIG. 8. ELITE marginal stability contour for a COMPASS-D 2.1 T discharge (full curve). The dashed and dotted curves show how the shear is predicted to vary as a function of α, assuming that the edge current density is dominated by bootstrap current: the dashed curve is for high collisionality ($\nu_* = 1.7$), while the dotted curve is for low collisionality ($\nu_* = 0.67$).

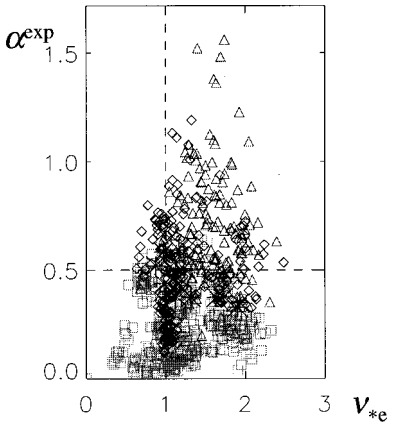

FIG. 9. The distribution of L- and H-mode discharges from measurements in COMPASS-D. The experimental measurement of $\alpha^{\exp} \equiv -2\mu_0 \times (R_0 q^2/B^2) dp/dr \simeq 3\alpha$ for this class of equilibria, where quantities are evaluated at the outboard mid-plane. Squares indicate the L-mode and diamonds (triangles) indicate the H-mode with (without) an ELM occurring during the data sampling.

expect an increase in ELM activity in the low collisionality discharges of larger tokamaks, rather than an inability to achieve a H-mode.

VI. DISCUSSION

Data on ELMs from DIII-D, supported by stability calculations from the low n MHD stability code GATO, suggest that a combination of both pressure and current density are responsible for the MHD precursors which are typically observed prior to an ELM. However, the higher toroidal mode numbers observed, up to $n \sim 9$, cannot be analyzed using GATO, and this has led to the development of a new edge MHD code, ELITE, for the analysis of moderate to high n edge-localized MHD instabilities. The code is designed to analyze peeling and ballooning modes, and their interaction. The H-mode is usually generated in a separatrix geometry and, in particular, all the experimental data we have discussed in this paper have been from plasmas with a separatrix. This makes a direct quantitative comparison of the existing ELITE stability code with experimental data difficult, because the edge localized modes are confined to the separatrix region. At present, ELITE cannot deal with the region close to the separatrix, because the straight field line angle used to generate the Fourier analysis becomes concentrated around the X-point; it is likely that this region will require a different treatment. Other physics which is likely to be important for a full MHD treatment of the plasma edge includes plasma flow and incorporating the boundary conditions associated with matching to the open field lines of the scrape-off layer, rather than directly to the vacuum. Nevertheless, this work is an important first step, which highlights a number of features associated with the coupled peeling–ballooning mode. Indeed, several of these features are in qualitative agreement with experiment: a role for both current and pressure to drive the instability, a role for collisionality and the bootstrap current, very localized (peeling limit) or relatively extended (ballooning limit) eigenmode structures which could account for the different ELM types observed, and the role of second stability access. These all motivate the further development of our model.

We have argued for the need to understand ELM phenomena in order to optimize the plasma performance, taking account of the need in a large tokamak to avoid large ELMs. Data from DIII-D suggests that large ELMs can be avoided by controlling the access to the second stability region (for ballooning modes), and a possible explanation for this has been proposed in terms of the greater radial extent predicted for ballooning modes when one is close to second-stable access. Indeed, experiments have already been performed on DIII-D where access to second stability, and therefore the ELM size, can be controlled by adjusting the plasma boundary shape.[24] Thus, plasmas with both high and low ''squareness'' have no second stability access, and small ELMs, while intermediate squareness discharges do typically have second stability access and large ELMs. The development of a code like ELITE will help in optimizing the plasma boundary so that the most dangerous MHD instabilities can be avoided, while maintaining a large edge temperature pedestal and the associated good confinement: this is the eventual goal.

ACKNOWLEDGMENTS

This work was supported by UK Department of Trade and Industry and Euratom, and U.S. Department of Energy under Contract No. DE-AC03-89ER51114 and Grant No. DE-FG03-95ER54309.

APPENDIX: ELITE MATRIX ELEMENTS

This appendix lists the matrix elements involved in Eqs. (10) and (11). Thus, we have

$$A_1^{m,m'}=(m-nq)\left[\frac{(m'-nq)}{q}T_1^{m,m'}-\frac{(m'-nq)}{n^2q^2}T_2^{m.m'}+2\frac{m'q'}{n^2q^2}T_3^{m,m'}\right.$$
$$+\left(\frac{m'q''}{n^2q^2}-2\frac{m'q'^2}{n^2q^3}\right)T_4^{m,m'}+i\frac{m'(m'-nq)}{n^2q}(2T_5^{m,m'}+T_8^{m,m'})-2i\frac{m'^2q'}{n^2q^2}T_6^{m,m'}$$
$$\left.+\frac{m'^2(m'-nq)}{n^2q}T_7^{m,m'}\right]-2\frac{qp'}{f}T_9^{m,m'}+\frac{m'qp'}{n}T_{11}^{m,m'},$$
$$A_2^{m,m'}=q'(m-nq)\left[2\frac{m'-nq}{nq}T_3^{m,m'}-2\frac{m'q'}{nq^2}T_4^{m,m'}-2i\frac{m'(m'-nq)}{nq}T_6^{m,m'}\right]-iqq'p'T_{10}^{m,m'},$$
$$A_3^{m,m'}=-\frac{q'^2(m-nq)(m'-nq)}{q}T_4^{m,m'},$$

where the T matrices are flux surface averages:

$$T_1^{mm'}=\oint\frac{f}{R^4B_p^2}e^{i(m-m')\omega}d\omega,\quad T_2^{mm'}=\oint\frac{qR^2B_p^2\nu''}{JB^2}e^{i(m-m')\omega}d\omega,$$
$$T_3^{mm'}=\oint\frac{B_p^2\nu'R^2}{JB^2}e^{i(m-m')\omega}d\omega,\quad T_4^{mm'}=\oint\frac{fB_p^2}{B^2}e^{i(m-m')\omega}d\omega,$$
$$T_5^{mm'}=\oint\frac{R^2B_p^2\nu'\omega'}{JB^2}e^{i(m-m')\omega}d\omega,\quad T_6^{mm'}=\oint\frac{fB_p^2\omega'}{B^2}e^{i(m-m')\omega}d\omega,$$
$$T_7^{mm'}=\oint\frac{fB_p^2\omega'^2}{B^2}e^{i(m-m')\omega}d\omega,\quad T_8^{mm'}=\oint\frac{fB_p^2\omega''}{B^2}e^{i(m-m')\omega}d\omega,$$
$$T_9^{mm'}=\oint\frac{\partial}{\partial\psi}\left(p+\frac{B^2}{2}\right)\frac{R^2}{B^2}e^{i(m-m')\omega}d\omega,\quad T_{10}^{mm'}=\oint\frac{\partial B^2}{\partial l}\frac{R^2B_p}{B^4}e^{i(m-m')\omega}d\omega,$$
$$T_{11}^{mm'}=\oint\frac{\partial B^2}{\partial l}\frac{\omega'R^2B_p}{B^4}e^{i(m-m')\omega}d\omega,\quad T_{12}^{mm'}=\oint e^{i(m-m')\omega}d\omega,\quad T_{13}^{mm'}=\oint\frac{1}{B^2}e^{i(m-m')\omega}d\omega.$$

In these definitions a prime denotes the differential with respect to poloidal flux, ψ, and J is the Jacobian of the orthogonal ψ, ϕ, χ coordinate system, where χ is a poloidal angle such that $J\,d\chi=dl/B_p$, $f=RB_\phi$ and

$$\nu=\frac{fJ}{R^2}.$$

[1]M. Kotschenreuther, W. Dorland, Q. P. Liu *et al.*, in *Proceedings of the 16th International Conference on Fusion Energy*, Montreal (International Atomic Energy Agency, Vienna, 1997), Vol. 2, p. 371.

[2]L. Lao, J. R. Ferron, R. L. Miller *et al.*, ''Effects of plasma shape and profiles on edge stability in DIII-D,'' to appear in *Proceedings of the 16th International Conference on Fusion Energy*, Yokohama (International Atomic Energy Agency, Vienna, 1998), Paper No. IAEA-F1-CN-69/EX8/1.

[3]L. C. Bernard, F. J. Helton, and R. W. Moore, Comput. Phys. Commun. **24**, 377 (1981).

[4]J. W. Connor, R. J. Hastie, and J. B. Taylor, Phys. Rev. Lett. **40**, 396 (1978).

[5]S. J. Fielding, J. D. Ashall, P. G. Carolan *et al.*, Plasma Phys. Controlled Fusion **38**, 1091 (1996).

[6]H. Zohm, Plasma Phys. Controlled Fusion **38**, 105 (1996).

[7]J. W. Connor, Plasma Phys. Controlled Fusion **40**, 531 (1998).

[8]T. H. Osborne and the DIII-D H-Mode Pedestal Study Group, in *Proceedings of the 24th European Physical Society Conference on Controlled Fusion and Plasma Physics*, Berchtesgaden (European Physical Society, Petit-Lancy, 1997), Part III, p. 1101.

[9]J. W. Connor, R. J. Hastie, H. R. Wilson, and R. L. Miller, Phys. Plasmas **5**, 2687 (1998).

[10]R. L. Miller, Plasma Phys. Controlled Fusion **40**, 753 (1998).

[11]D. Lortz, Nucl. Fusion **15**, 49 (1975).

[12]J. Manickam, Phys. Fluids B **4**, 1901 (1992).

[13]J. W. Connor, R. J. Hastie, and J. B. Taylor, Proc. R. Soc. London, Ser. A **365**, 1 (1979).

[14]C. Mercier, Nucl. Fusion **1**, 47 (1960); Nucl. Fusion Suppl. **2**, 801 (1962).

[15]H. R. Wilson, J. W. Connor, A. R. Field, S. J. Fielding, R. J. Hastie, R. L. Miller, and J. B. Taylor, ''Influence of the plasma edge on tokamak performance,'' to appear in Nucl. Fus. (1999).

[16]H. R. Wilson and R. L. Miller, Phys. Plasmas **6**, 873 (1999).

[17]A. Pletzer (private communication, 1998).

[18]C. M. Bishop, P. Kirby, J. W. Connor, R. J. Hastie, and J. B. Taylor, Nucl. Fusion **24**, 1579 (1984).

[19]R. L. Miller, M. S. Chu, J. M. Greene, Y. R. Lin-Liu, and R. E. Waltz, Phys. Plasmas **5**, 973 (1998).

[20]S. J. Fielding, A. R. Field, C. Hunt *et al.*, ''H-modes on COMPASS-D with high power ECRH,'' to appear in *Proceedings of the 25th European Physical Society Conference on Controlled Fusion and Plasma Physics*, Prague (European Physical Society, Petit-Lancy, Switzerland, 1998).
[21]*Technical Basis for the ITER Interim Design Report, Cost Review and Safety Analysis* (International Atomic Energy Agency, Vienna, 1996).
[22]A. W. Morris, S. J. Fielding, M. Valovic *et al.*, ''Improved confinement, high β regimes and edge behavior on the COMPASS-D tokamak with high power ECRH and LHCD'' to appear in Ref. 2, Paper No. IAEA-F1-CN-69/EXP2/04.
[23]A. R. Field, P. G. Carolan, N. J. Conway, and M. G. O'Mullane, Rev. Sci. Instrum. **70**, 355 (1999).
[24]J. R. Ferron, L. L. Lao, R. L. Miller, T. H. Osborne, B. W. Rice, E. J. Strait, and T. S. Taylor, ''Modification of tokamak edge instability character through control of ballooning mode second stability accessibility,'' General Atomics Report GA-A22974, submitted to Nucl. Fusion.